# Spectral functions in Minkowski quantum electrodynamics from neural reconstruction: Benchmarking against dispersive Dyson–Schwinger integral equations

Rodrigo Carmo Terin<sup>1,\*</sup>

<sup>1</sup>King Juan Carlos University, Facuty of Experimental Sciences and Technology, Department of Applied Physics, Av. del Alcalde de Móstoles, 28933, Madrid, Spain

A Minkowskian physics-informed neural network approach (M-PINN) is formulated to solve the Dyson–Schwinger integral equations (DSE) of quantum electrodynamics (QED) directly in Minkowski spacetime. Our novel strategy merges two complementary approaches: (i) a dispersive solver based on Lehmann representations and subtracted dispersion relations, and (ii) a M-PINN that learns the fermion mass function  $B(p^2)$ , under the same truncation and renormalization configuration (quenched, rainbow, Landau gauge) with the loss integrating the DSE residual with multiscale regularization, and monotonicity/smoothing penalties in the spacelike branch in the same way as in our previous work in Euclidean space. The benchmarks show quantitative agreement from the infrared (IR) to the ultraviolet (UV) scales in both on-shell and momentum-subtraction schemes. In this controlled setting, the M-PINN reproduces the dispersive solution whilst remaining computationally compact and differentiable, paving the way for extensions with realistic vertices, unquenching effects, and uncertainty-aware variants.

### I. INTRODUCTION

The Dyson–Schwinger equations (DSEs) furnish a nonperturbative continuum approach to the Green functions of any quantum field theories (QFTs). Arising from the seminal works of Dyson and Schwinger in the late 1940s and early 1950s [1–3], the DSEs define an infinite tower of coupled integral equations for all *n*-point functions. Their works have become fundamental to understanding dynamical mass generation, confinement, and critical phenomena in strongly interacting systems [4–7].

In QED, the fermion and photon propagator equations occupy an important role in analyzing the interplay between gauge invariance, chiral symmetry, and renormalization. Because the complete DSE hierarchy is intractable, truncations are unavoidable. The Rainbow–Ladder approximation, where the dressed vertex is replaced by its bare form, gives a baseline for dynamical mass generation [8–12]. More refined schemes employ the Ball–Chiu [13] or Curtis–Pennington [14, 15] vertices, which impose the so-called Ward–Takahashi identities (WTIs). These truncations remain widely used as benchmarks for gauge-consistent calculations, even in contemporary applications [16–19]. Such truncations have been proven predictive in multiple situations. In quantum chromodynamics (QCD), DSEs studies have clarified the emergence of an effective gluon mass scale [16, 20], the infrared behavior of Green functions [5, 21], and the properties of mesons and baryons through Bethe–Salpeter and Faddeev equations [4, 22–24]. In QED, analogous methods describe dynamical fermion mass generation [8, 11] and reveal how the vertex structure influences the solution space [12, 18]. These results call attention to the necessity of symmetry-preserving approximations for meaningful nonperturbative predictions.

In this context, the extension from Euclidean space to Minkowskian space-time introduces additional challenges. Analytic continuation is often obstructed by singularities, thresholds, and branch cuts along the real axis [25–27]. Direct Minkowski solutions therefore require explicit dispersive techniques. In the literature there is a work that introduced a framework that mixed Lehmann spectral representations with momentum subtraction scheme (MOM) renormalization, enabling DSEs to be solved directly in Minkowski space-time [28]. In this setting, subtraction on a fixed scale yields integral equations valid in both time- and space-like regions, allowing explicit comparison with Euclidean formulations and exposing controlled discrepancies at strong coupling [29, 30]. Spectral representations also connect directly to confinement diagnostics and in nonconfining theories, positivity guarantees the existence of Lehmann representations for propagators, and their absence signals confinement [31, 32]. Earlier analysis made this criterion operational: beyond a critical coupling, the spectral solution ceases to exist, corresponding with the onset of a confined phase [28]. The spectral approach thus links analyticity, renormalization, and dynamical phases in a unified way.

Indeed, for gauge theories, the implementation of WTIs is non-negotiable, the longitudinal component of the fermion-photon vertex is fixed by the Ball-Chiu construction [13], implying the equality  $Z_1 = Z_2$  between vertex

<sup>\*</sup> rodrigo.carmo@urjc.es

and fermion renormalization constants. Likewise, the vacuum polarization must remain transverse to preserve gauge covariance. Approaches, e.g., the Pinch technique [33, 34] and the background field method [35] give complementary routes to building up gauge-independent quantities. Within this dispersive program, the Landau gauge and rainbow truncation already furnish a controlled environment for exploring these constraints. A more systematic description was given by us in the work [36], where we derived the QED DSEs tower in Minkowskian spacetime together with WTIs for the fermion–photon and two-photon–two-fermion irreducible vertices.

In parallel, machine learning (ML) algorithms have emerged as alternative solvers for operator equations. The PINNs [37–39] incorporate residuals of fundamental differential equations into the loss function, enabling solutions consistent with fundamental physics. Applications range in many domains, including fluid dynamics [40], cardiovascular modelling [41], plasma turbulence [42], quantum chemistry [43], and molecular dynamics [44]. Extensions, for instance, Bayesian PINNs [45], XPINNs [46], DeepONets [47], and multifidelity strategies [48] further expand their scope, allowing scalability and uncertainty quantification [49, 50]. Additionally, a novel study [51] has shown that PINNs discovered new families of unstable singularities in nonlinear flow equations. The approach of the authors mixes mathematical structure with ML accuracy, showing how the latter can reveal hidden patterns in complex physical systems. This goes in the same direction as we have done recently, when we applied PINNs to Euclidean QED DSEs [52], directly minimizing integral-equation residuals to recover continuous fermion dressing functions. A multiscale loss with IR, intermediate, and UV windows proved fundamental to stabilize training and guarantee perturbative asymptotics, establishing a practical onset for learning nonlocal integral equations in QFTs with physically motivated regularization. In the present work we extend this program to Minkowski space-time through two supportive strategies: (i) a dispersive baseline inspired by Ref. [28], solving for spectral densities with MOM subtractions; and (ii) a PINN trained directly on the real axis (complex-valued outputs). With a common truncation, gauge, and subtraction point, we enable a transparent comparison to assess the stability and consistency of neural solvers in Minkowskian kinematics and their capacity to capture dynamical mass generation in the time-like domain.

Methodologically, this study assumes two design principles from our earlier works. From our Euclidean PINN approach [52], we retain the residual-based multiscale loss with a perturbative UV constraint. From our gauge-invariant neural network (GINN) framework [53], we import the notion of gauge parameters as kernel selectors and WTIs as stabilizing constraints. Together, these guide the construction of a Minkowskian PINN loss that mirrors subtracted dispersion relations, with the dispersive solver serving as a benchmark recognized by the DSEs community.

This paper is organized as follows. Section II sets the Minkowskian background and spectral formulation, fixing notation, renormalization conditions, and the dispersion–relation framework used as benchmark. Section III details the two complementary solvers: the dispersive DSE algorithm (spectral equations, principal–value treatment, reconstruction of B) and our M-PINN formulation (network design, residual-based loss with multi-scale terms, and spacelike monotonicity/smoothing). Results for spacelike and timelike kinematics are presented and discussed within the same gauge/truncation setup and renormalization scheme. Lastly, Section IV summarizes the main findings, compares on-shell vs. MOM schemes, comments on the analytic structure, and outlines extensions to dressed vertices, unquenching, and uncertainty-aware variants.

## II. BACKGROUND AND SPECTRAL FORMULATION

From now on we follow the notation and conventions of one of our previous works [36], and at the same time taking the dispersive program of [28] as a benchmark for our Minkowskian analysis. The renormalized fermion propagator in this well-known spacetime signature is parameterized as

$$S^{-1}(p) = A(p^2) \not p - B(p^2), \qquad (1)$$

where  $A(p^2)$  and  $B(p^2)$  are fermion dressing functions. In quenched rainbow truncation and Landau gauge, the DSE takes the form

$$S^{-1}(p) = \not p - m_0 - ie^2 \int \frac{d^4k}{(2\pi)^4} \gamma^{\mu} S(p-k) \gamma^{\nu} D_{\mu\nu}(k) , \qquad (2)$$

with bare vertex  $\Gamma^{\mu} = \gamma^{\mu}$  and photon propagator  $D_{\mu\nu}(k)$ . Gauge-covariant vertex constructions such as Ball–Chiu and Curtis–Pennington [13, 14] guarantee obedience with WTIs, but the rainbow setup already gives a consistent minimal onset.

Renormalization requires explicit subtraction conditions. In the MOM scheme, subtractions are imposed on a fixed scale  $\mu$  to warranty finite, physically meaningful propagators. WTIs implement  $Z_1 = Z_2$ , while  $Z_3$  renormalizes the photon field. In Landau gauge, these relations simplify, but MOM subtractions remain essential. When asymptotic

states exist, the fermion propagator admits a Lehmann representation,

$$S(p) = \int_{s_0}^{\infty} ds \, \frac{\rho_s(s) + \not p \, \rho_v(s)}{p^2 - s + i\epsilon} \,, \tag{3}$$

with spectral weights  $\rho_{s,v}(s)$ . The scalar/vector decomposition of the fermion self-energy yields dispersion relations for the dressing functions,

$$A(p^2) = Z_2 - \int_{s_0}^{\infty} ds \, \frac{\rho_v(s)}{p^2 - s + i\epsilon},\tag{4}$$

$$B(p^2) = Z_m m(\mu) - \int_{s_0}^{\infty} ds \, \frac{\rho_s(s)}{p^2 - s + i\epsilon},\tag{5}$$

so that the dynamical mass function

$$M(p^2) = \frac{B(p^2)}{A(p^2)} \tag{6}$$

is renormalization–group invariant. Positivity of  $\rho_{s,v}$  signals deconfinement, and its loss correlates with confinement. Gauge invariance requires the photon polarization tensor to be transverse,

$$\Pi^{\mu\nu}(q) = \left(g^{\mu\nu} - \frac{q^{\mu}q^{\nu}}{q^2}\right)\Pi(q^2), \qquad q_{\mu}\Pi^{\mu\nu}(q) = 0.$$
 (7)

Its renormalized form in MOM is given by a once–subtracted dispersion relation,

$$\Pi_R(q^2, \mu^2) = \int_{s_0}^{\infty} ds \, \rho_{\gamma}(s) \left[ \frac{1}{q^2 - s + i\epsilon} - \frac{1}{\mu^2 - s + i\epsilon} \right],\tag{8}$$

with  $\rho_{\gamma}(s)$  the photon spectral density. The renormalized Landau–gauge propagator then reads

$$D_{\mu\nu}(q) = \frac{-i}{q^2 \left[1 - \Pi_R(q^2, \mu^2)\right]} \left(g_{\mu\nu} - \frac{q_\mu q_\nu}{q^2}\right). \tag{9}$$

In weak coupling, the positivity of  $\rho_{\gamma}$  corresponds to a massless photon. In stronger coupling, loss of positive solutions means dynamical mass generation or confinement.

Compared to Euclidean space, the Minkowskian formulation introduces branch cuts, thresholds, and singularities on the real axis. Naive Wick rotation is obstructed, and discrepancies between both solutions emerge at strong coupling. It is well established that the fermion propagator in massless QED may lose its timelike pole entirely, a phenomenon interpreted as evidence for confinement. The dispersive formulation confirmed that the absence of Lehmann solutions correlates with the onset of strong coupling. Related insights into nonlocality and spectral positivity were emphasized in nonlocal field theory [32]. Altogether, the dispersive/MOM framework gives both a well-defined renormalization scheme and a diagnostic of confinement and analyticity. In what follows we take it as baseline for comparison with our M-PINN solvers.

### III. TRADITIONAL AND PINN METHODS FOR MINKOWSKIAN SPACE-TIME

In order to benchmark our M-PINNs, we implement a self-contained dispersive solver based on the spectral representation of the fermion propagator. In kinematic regimes where asymptotic states exist, one uses Eq. (3) so that the inverse propagator decomposes as in Eq. (1). In Landau gauge with a rainbow vertex, inserting this ansatz into the DSE gives a coupled system of real integral equations for the spectral functions  $\sigma_v(\omega)$  and  $\sigma_s(\omega)$ :

$$\sigma_v(\omega) = \frac{3\alpha}{4\pi} \int_0^\infty d\omega' \, \rho_s(\omega') \, K_v(\omega, \omega'), \tag{10}$$

$$\sigma_s(\omega) = \frac{3\alpha}{4\pi} \int_0^\infty d\omega' \, \rho_s(\omega') \, K_s(\omega, \omega') \,, \tag{11}$$

with kernels

$$K_{v}(\omega,\omega') = \frac{1}{\omega} \left[ \theta(\omega - \omega') - \frac{\omega'}{\omega - \omega'} \right], \tag{12}$$

$$K_s(\omega, \omega') = \frac{m}{\omega} \left[ \theta(\omega - \omega') - \frac{\omega}{\omega - \omega'} \right]. \tag{13}$$

The absorptive parts  $\rho_{v,s}(\omega)$  follow by simple quadratures. In particular, the scalar density is

$$\rho_s(\omega) = -\frac{3\alpha}{4\pi} m \left(1 - \frac{m^2}{\omega}\right) + \int_0^\omega d\omega' \, \sigma_s(\omega') - \omega \int_0^\omega d\omega' \, \frac{\sigma_s(\omega')}{\omega'} \,, \tag{14}$$

with an analogous expression for  $\rho_v(\omega)$ . Once  $\rho_{v,s}$  are known, the dressing functions are reconstructed by subtracted dispersion relations. For the vector component

$$A(p^2) = 1 + \frac{p^2 - \mu^2}{\pi} \int_0^\infty d\omega \, \frac{\rho_v(\omega)}{(\omega - \mu^2)(\omega - p^2)} \,, \tag{15}$$

while the scalar component reads

$$B(p^2) = m(\mu) + \frac{p^2 - \mu^2}{\pi} \int_0^\infty d\omega \, \frac{\rho_s(\omega)}{(\omega - \mu^2)(\omega - p^2)} \,. \tag{16}$$

The subtraction guarantees UV convergence and fixes  $B(\mu^2) = m(\mu)$  by construction, completing the dispersive reconstruction of the Minkowski–space solution given by Eqs. (15) and (16). In practice, we discretize the timelike spectral variable on a logarithmic grid  $\omega_i \in [s_0, \omega_{\text{max}}]$  with  $N_\omega \sim 10^3$ , and solve the unitary equations for  $\sigma_{v,s}(\omega_i)$  iteratively. Cauchy principal values are handled by removing a neighborhood  $\eta$  around each singularity and combining the evaluations at  $\eta$  and  $\eta/2$  using Richardson extrapolation to reduce bias [54, 55]. Convergence is declared once  $\max\{\|\Delta\sigma_v\|_\infty, \|\Delta\sigma_s\|_\infty\} < 10^{-7}$ . We then compute  $\rho_s(\omega)$  from Eq. (14) and reconstruct  $B(p^2)$  from Eq. (16). Finally, we evaluate  $B(p^2)$  on real spacelike  $(p^2 < 0)$  and timelike  $(p^2 > 0)$  grids using trapezoidal quadrature and on–shell MOM renormalization,  $\mu^2 = m^2$  with  $m(\mu) = 1$ .

We now describe our PINN viewpoint already tested in [52] for Euclidean QED DSEs to tackle the same problem in the Minkowskian signature under the same truncation and renormalization used above (Landau gauge, rainbow vertex, quenched photon). Since  $A(p^2) \approx 1$  at leading order, the dynamical mass is  $M(p^2) = B(p^2)$  and we focus the network on learning B. Our M-PINN approximates the map  $p^2 \mapsto B(p^2)$  with a neural network (NN)  $B_\theta$  trained by minimizing a residual loss that represents the rainbow equation reduced to a one-dimensional integral split at  $p^2$ :

$$\mathscr{R}[B](p^2) = B(p^2) - \frac{3\alpha}{4\pi} \left[ \int_0^{p^2} dk^2 \frac{B(k^2)}{k^2 + B^2(k^2)} \frac{k^2}{p^2} + \int_{p^2}^{\kappa^2} dk^2 \frac{B(k^2)}{k^2 + B^2(k^2)} \right] = 0, \tag{17}$$

with  $\kappa^2$  the UV box (set to 1 in dimensionless units). We work on log-grids and use as input  $x = \log_{10}(|p^2|)$ . For the timelike branch we augment x with Fourier features to capture the mild UV wiggles; for spacelike we use a plain multilayer perceptron (MLP). Also, we use two small networks with the same depth/width (5 layers, width 96) and the timelike net concatenates 32 pairs of Fourier features to x; the spacelike net receives only x. Both output a scalar  $B_{\theta}(x)$ . In this way, the loss is given by:

$$\mathcal{L}_{\text{phys}} = \langle \mathscr{R}[B_{\theta}]^2 \rangle, \tag{18}$$

$$\mathcal{L}_{\text{data}}^{\text{TL/SL}} = \langle (B_{\theta} - B_{\text{trad}})^2 \rangle,$$
 (19)

$$\mathcal{L}_{\text{reg}}^{\text{mid}} = \left\langle \left[ \log(1 + |B_{\theta}|) - \log(1 + |B_{\text{trad}}|) \right]^2 \right\rangle_{\text{mid}}, \tag{20}$$

$$\mathcal{L}_{\text{reg}}^{\text{high}} = \left\langle \left[ \log(1 + |B_{\theta}|) - \log(1 + |B_{\text{trad}}|) \right]^2 \right\rangle_{\text{high}}, \tag{21}$$

$$\mathcal{L}_{\text{tail}} = \langle (B_{\theta} - B_{\text{UV}})^2 \rangle_{\text{UV}}, \tag{22}$$

$$\mathcal{L}_{\text{cont}}^{\text{TL}} = \left(B_{\theta}(p_{-}^2) - B_{\theta}(p_{+}^2)\right)^2, \tag{23}$$

$$\mathcal{L}_{\rm ir}^{\rm TL} = \langle (\Delta_{\rm log} B_{\theta})^2 \rangle_{\rm IR}, \tag{24}$$

$$\mathcal{L}_{\rm SL}^{\rm mono} = \langle \text{ReLU}(dB_{\theta}/d\log|p^2|) \rangle,$$
 (25)

$$\mathcal{L}_{\rm SL}^{H^1} = \langle (\Delta_{\rm log} B_{\theta})^2 \rangle. \tag{26}$$

with

$$\mathcal{L}_{\mathrm{TL}} = w_{\mathrm{phys}} \mathcal{L}_{\mathrm{phys}} + w_{\mathrm{data}}^{\mathrm{TL}} \mathcal{L}_{\mathrm{data}}^{\mathrm{TL}} + w_{\mathrm{mid}} \mathcal{L}_{\mathrm{reg}}^{\mathrm{mid}} + w_{\mathrm{high}} \mathcal{L}_{\mathrm{reg}}^{\mathrm{high}} + w_{\mathrm{cont}} \mathcal{L}_{\mathrm{cont}}^{\mathrm{TL}} + w_{\mathrm{ir}} \mathcal{L}_{\mathrm{ir}}^{\mathrm{TL}} + w_{\mathrm{tail}} \mathcal{L}_{\mathrm{tail}}, \tag{27}$$

$$\mathcal{L}_{\mathrm{SL}} = w_{\mathrm{phys}} \mathcal{L}_{\mathrm{phys}} + w_{\mathrm{data}}^{\mathrm{SL}} \mathcal{L}_{\mathrm{data}}^{\mathrm{SL}} + w_{\mathrm{mid}} \mathcal{L}_{\mathrm{reg}}^{\mathrm{mid}} + w_{\mathrm{high}} \mathcal{L}_{\mathrm{reg}}^{\mathrm{high}} + w_{\mathrm{tail}} \mathcal{L}_{\mathrm{tail}} + w_{\mathrm{mono}} \mathcal{L}_{\mathrm{SL}}^{\mathrm{mono}} + w_{H^{1}} \mathcal{L}_{\mathrm{SL}}^{H^{1}}.$$
 (28)

and, finally

$$B_{\rm UV}(p^2) = \beta - \gamma \log(1 + |p^2|) + \mathbf{1}_{\rm TL} a \sin(\omega \log(1 + |p^2|)),$$
 (29)

where,  $\mathscr{L}_{\text{phys}}$  is the mean squared residual of the reduced DSE (17). The data terms  $\mathscr{L}_{\text{data}}^{\text{TL/SL}}$  align  $B_{\theta}$  with the dispersive benchmark on the timelike (TL)/spacelike (SL) grids. The log-window terms  $\mathscr{L}_{\text{reg}}^{\text{mid}}$  and  $\mathscr{L}_{\text{reg}}^{\text{high}}$  compare  $\log(1+|B|)$  in mid and high momentum windows, stabilizing the UV shape over many orders in  $p^2$ . The UV template loss  $\mathscr{L}_{\text{tail}}$  anchors  $B_{\theta}$  to the form (29); only in TL we include one sinusoidal mode in  $\log p^2$  to capture mild wiggles. For TL we also add a continuity penalty at the tail-gluing point,  $\mathscr{L}_{\text{cont}}^{\text{TL}}$ , and an IR smoothing term  $\mathscr{L}_{\text{ir}}^{\text{TL}}$  (second differences on the log grid). For SL we impose nonincreasing behavior with  $\mathscr{L}_{\text{SL}}^{\text{mono}}$  and add smoothness with the  $H^1$  penalty  $\mathscr{L}_{\text{SL}}^{H^1}$ . In addition, the same weights are used for all couplings (no ad hoc reweighting) and we use deterministic per- $\alpha$  initialization for reproducibility (same pseudo-random number generator (PRNG) seed per coupling) and optimize with Adam (10<sup>-3</sup>, 6000 epochs); TL and SL networks are trained independently.

For clarity we present each regime in a separate figure. Fig 1 compares PINN (left) and dispersive (right) in the spacelike domain, and Fig. 2 shows the timelike domain with superposed curves. We observe uniform agreement from IR to UV; the TL tail is stabilized by the logarithmic template with one sine mode, and in SL the combination monotonicity+ $H^1$  together with deterministic initialization removes the small drift seen in stochastic runs.

In these figures, spacelike curves are shown as B vs.  $-p^2$ . For the timelike panel we apply only a simple transform

$$B_{\text{plot}}(p^2) = \frac{B(p^2) + B_0}{S},$$
 (30)

where  $B_0$  is chosen so that the global minimum becomes 0, and S is chosen so that the global maximum maps to 1.2. Because the dispersion relations are written with a subtraction, the ultraviolet behavior of  $B(p^2)$  follows a logarithmic self–energy,  $B(p^2) \simeq m(\mu) \left[1 - c \alpha \ln(p^2/\mu^2)\right]$  with c > 0, e.g., changing the subtraction point only shifts Re B vertically in the timelike panel.

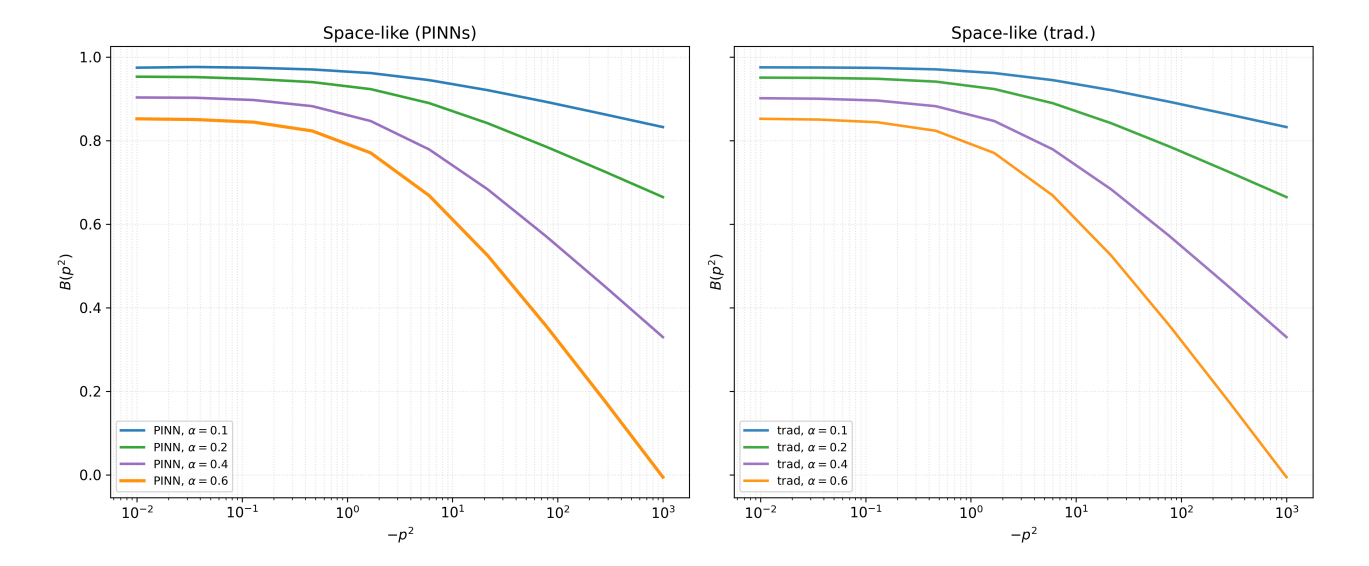


Figure 1: Comparison among PINNs (left) and the traditional dispersive Dyson–Schwinger solver (right) for the scalar dressing  $B(p^2)$  in the spacelike regime. All curves use  $\mu^2 = m^2$  and the normalization  $B(p^2)$ .

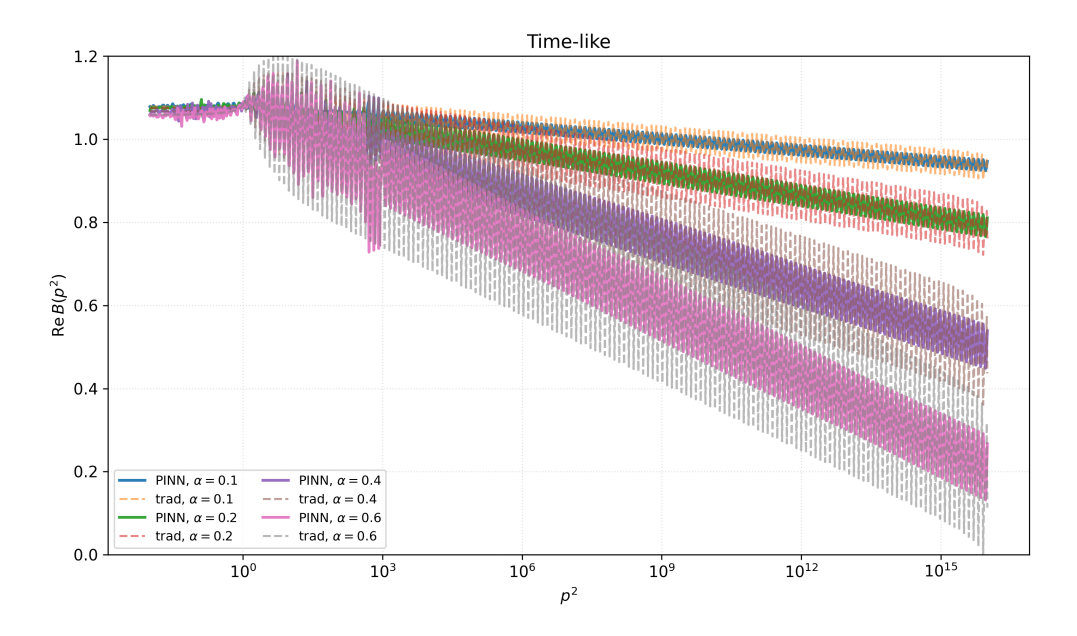


Figure 2: Comparison between M-PINNs and the traditional dispersive Dyson–Schwinger solver for the real part of the mass function  $B(p^2)$  in the timelike regime. All curves use  $\mu^2 = m^2$  and the normalization  $B(p^2)$ .

Here we summarize everything by comparing both viewpoints where the first is the traditional dispersive solver, in which the fermion propagator is reconstructed from spectral densities using subtracted dispersion relations; its equations are discretized on a logarithmic grid and solved iteratively, with principal–value singularities handled by Richardson extrapolation as previously mentioned. Convergence is declared once successive updates differ below a fixed tolerance. Also, this approach guarantees analyticity and causality by construction, but its output is limited to discrete grid points and the computational cost can increase quickly with grid refinement. The second is our M-PINN framework, where the dynamical mass function  $B(p^2)$  is represented as a smooth continuous function learned by a NN. Instead of point–by–point iterations, the solution is obtained by minimizing a residual–based loss that includes multi–scale penalties in the IR, intermediate and UV regions. Additional constraints are used in each branch: Fourier features for the timelike side to capture oscillatory tails, and monotonicity plus smoothing terms for the spacelike side. Optimization is performed globally with gradient descent, producing a differentiable solution valid over the full momentum range.

Last but not least, it is important to point out that nonperturbative dynamics in gauge theories can be investigated through two main paradigms: continuum functional equations and lattice Monte Carlo simulations [56–58]. The former, exemplified by the DSEs, represent exact relations among Green functions that can be solved under controlled truncations and renormalization conditions. The latter reformulates the theory on a discrete Euclidean grid, where the path integral is estimated stochastically from large ensembles of field configurations. Both frameworks aim to capture the same fundamental principles beyond perturbation theory, however they differ deeply in methodology: DSEs give analytic and continuous solutions in momentum space, while lattice simulations yield statistical ensembles of correlators defined at discrete points.

In this context, NNs offer a unifying and more flexible framework. When informed by the DSE residuals, they act as deterministic solvers that minimize functional discrepancies directly in the continuum, producing smooth propagators and spectral functions that preserve analyticity and causality. On the contrary, when trained on lattice data [59], the same architectures can learn statistical correlations or reconstruct spectral densities from Euclidean correlators, effectively bypassing the ill-posed analytic continuation problem. In both cases, the neural representation interpolates between regimes that are traditionally disconnect, analytical (DSE) and statistical (lattice), showing that deep NNs can connect first-principles simulations and functional formulations within a single computational paradigm. From a methodological viewpoint, this flexibility makes NNs more general than both Monte Carlo sampling and fixed-grid quadratures. Whereas lattice methods are limited to Euclidean space and require stochastic sampling, and quadratures rely on discretized kernels that scale poorly with dimensionality, the neural formulation handles arbitrary resolutions, guarantees physical symmetries through the loss function, and yields differentiable solutions over the entire momentum domain. In this sense, PINNs extend traditional continuum approaches and at the same time remain compatible with lattice data assimilation, suggesting that neural solvers can serve as a common language between functional and

statistical nonperturbative approaches.

### IV. CONCLUSIONS AND OUTLOOK

We presented a Minkowskian formulation of physics-informed machine learning for Dyson–Schwinger integral equations and validated it against a traditional dispersive benchmark. Working in quenched rainbow QED and Landau gauge, the spectral solver gives a reference built from subtracted dispersion relations, and at the same time the M-PINN learns the scalar dressing  $B(p^2)$  by minimizing a residual that mirrors the one-dimensional split of the rainbow equation. The training includes multi-scale (IR/intermediate/UV) weighting, a simple perturbative UV template. The figures show that the M-PINN reproduces the dispersive solution throughout the full momentum domain for all tested couplings  $\alpha \in \{0.1, 0.2, 0.4, 0.6\}$ , with consistent renormalization ( $\mu^2 = m^2$ ). The timelike branch, including the gentle UV oscillations, is captured through Fourier features in  $\log p^2$ , while the spacelike decay is stabilized by the monotonicity and smoothing terms. The analytic structure (peaks near threshold and the overall cut) remains consistent with the dispersive reconstruction.

The present work also point up concrete next steps. First, the truncation is minimal (rainbow, quenched,  $A(p^2) \approx 1$ ). Incorporating symmetry-preserving vertices (Ball–Chiu or Curtis–Pennington) and photon propagator will test gauge covariance more rigorously. Second, our UV template could be replaced by tails motivated by the renormalization group, ensuring asymptotic control. Third, while we compared on-shell and MOM schemes, a systematic study of system dependence and of strong-coupling regimes near the loss of Lehmann positivity is still needed. Finally, uncertainty quantification and scalability can be addressed with Bayesian PINNs and XPINNs, and the same mechanism can be extended to the famous Bethe–Salpeter equations [60] for bound states. In summary, the dispersive solver and the M-PINN agree quantitatively in Minkowskian kinematics under identical supositions, showing that residual-based neural solvers can handle nonlocal integral equations with realistic renormalization. We expect this combination of spectral baselines and PINNs to give a practical route toward gauge-consistent, uncertainty-aware computations of propagators and amplitudes directly on the real axis.

Lastly, taken together, our Euclidean PINN results [52], the stochastic QED-NN mapping [53], and the present Minkowskian benchmark constitute a threefold program: stability criteria (gain  $\leftrightarrow$  Lehmann positivity), gauge covariance (WTIs  $\leftrightarrow$  kernel design), and analytic continuation (Euclidean  $\leftrightarrow$  Minkowski). This unified perspective suggests systematic extensions to QCD, scalar Yukawa models, and symmetry-preserving truncations.

#### ACKNOWLEDGMENTS

R.C. Terin thanks Vladimír Šauli for sending a helpful reference.

<sup>[1]</sup> Freeman J. Dyson. The s matrix in quantum electrodynamics. *Phys. Rev.*, 75:1736–1755, 1949. doi 10.1103/PhysRev.75.1736.

<sup>[2]</sup> Julian Schwinger. On the green's functions of quantized fields. Proc. Natl. Acad. Sci. USA, 37:452–455, 1951. doi: 10.1073/pnas.37.7.452.

<sup>[3]</sup> Julian Schwinger. On the green's functions of quantized fields ii. Proc. Natl. Acad. Sci. USA, 37:455–459, 1951. doi: 10.1073/pnas.37.7.455.

<sup>[4]</sup> Craig D. Roberts and Anthony G. Williams. Dyson–schwinger equations and their application to hadronic physics. *Prog. Part. Nucl. Phys.*, 33:477–575, 1994. doi:10.1016/0146-6410(94)90049-3.

<sup>[5]</sup> Reinhard Alkofer and Lorenz von Smekal. The infrared behavior of qcd green's functions. *Phys. Rept.*, 353:281–465, 2001. doi:10.1016/S0370-1573(01)00010-2.

<sup>[6]</sup> Craig D. Roberts and Sebastian M. Schmidt. Dyson-schwinger equations: Density, temperature and continuum strong qcd. Prog. Part. Nucl. Phys., 45:S1-S103, 2000. doi:10.1016/S0146-6410(00)90011-5.

<sup>[7]</sup> Christian S. Fischer. Qcd at finite temperature and chemical potential from dyson–schwinger equations. *Prog. Part. Nucl. Phys.*, 105:1–60, 2019. doi:10.1016/j.ppnp.2019.01.002.

<sup>[8]</sup> D. Atkinson, P. W. Johnson, and P. Maris. Dynamical chiral symmetry breaking with an infrared dominant vertex. Phys. Rev. D, 42:602–609, 1990. doi:10.1103/PhysRevD.42.602.

<sup>[9]</sup> P. Maris, C. D. Roberts, and P. C. Tandy. Pion mass and decay constant. *Phys. Lett. B*, 420:267–273, 1998. doi: 10.1016/S0370-2693(97)01535-9.

<sup>[10]</sup> Christian S. Fischer, Reinhard Alkofer, Tobias Dahm, and Peter Maris. Dynamical chiral symmetry breaking in unquenched qed<sub>3</sub>. *Phys. Rev. D*, 70:073007, 2004. doi:10.1103/PhysRevD.70.073007.

- [11] E. Rojas, A. Ayala, A. Bashir, and A. Raya. Dynamical mass generation in qed with magnetic fields. *Phys. Rev. D*, 77: 093004, 2008. doi:10.1103/PhysRevD.77.093004.
- [12] Ayse Kızılersu, Tom Sizer, Michael R. Pennington, Anthony G. Williams, and Richard Williams. Reconstructing the fermion–photon vertex in strongly coupled gauge theories. *Phys. Rev. D*, 91(6):065015, 2015. doi: 10.1103/PhysRevD.91.065015.
- [13] J. S. Ball and T.-W. Chiu. Analytic properties of the vertex function in gauge theories. i. Phys. Rev. D, 22:2542–2549, 1980. doi:10.1103/PhysRevD.22.2542.
- [14] David C. Curtis, Michael R. Pennington, and D. A. Walsh. On the gauge dependence of dynamical fermion masses. *Phys. Lett. B*, 249:528–532, 1990. doi:10.1016/0370-2693(90)91005-3.
- [15] David C. Curtis and Michael R. Pennington. Nonperturbative truncation of the schwinger-dyson equations. Phys. Rev. D, 44:536-539, 1991. doi:10.1103/PhysRevD.44.536.
- [16] John M. Cornwall. Dynamical mass generation in continuum qcd. Phys. Rev. D, 26:1453–1478, 1982. doi 10.1103/PhysRevD.26.1453.
- [17] William J. Marciano and Heinz Pagels. Quantum chromodynamics: A review. Phys. Rept., 36:137–276, 1978. doi: 10.1016/0370-1573(78)90208-9.
- [18] Adnan Bashir, Ayse Kızılersu, and Michael R. Pennington. Gauge independent solutions to the fermion propagator dyson-schwinger equation. *Phys. Rev. D*, 57:1242–1248, 1998. doi:10.1103/PhysRevD.57.1242.
- [19] Victor M. B. Guzmán and Adnan Bashir. Constraining the transverse structure of the fermion–photon vertex in qed. *Phys. Rev. D*, 107(7):073008, 2023. doi:10.1103/PhysRevD.107.073008.
- [20] A. C. Aguilar, A. A. Natale, and P. S. Rodrigues da Silva. Relating a gluon mass scale to an infrared fixed point in pure gauge qcd. *Phys. Rev. Lett.*, 90:152001, 2003. doi:10.1103/PhysRevLett.90.152001.
- [21] Markus Q. Huber. Nonperturbative properties of yang-mills theories. *Phys. Rept.*, 879:1–92, 2020. doi: 10.1016/j.physrep.2020.04.004.
- [22] P. Maris and P. C. Tandy. Bethe–salpeter study of vector meson masses and decay constants. Phys. Rev. C, 60:055214, 1999. doi:10.1103/PhysRevC.60.055214.
- [23] Gernot Eichmann, Helios Sanchis-Alepuz, Richard Williams, Reinhard Alkofer, and Christian S. Fischer. Baryons as relativistic three-quark bound states. *Prog. Part. Nucl. Phys.*, 91:1–100, 2016. doi:10.1016/j.ppnp.2016.07.001.
- [24] Minghui Ding, Craig D. Roberts, and Sebastian M. Schmidt. Emergence of hadron mass and structure. *Particles*, 6(1): 57–120, 2023. doi:10.3390/particles6010005.
- [25] M. Gimeno-Segovia and F. J. Llanes-Estrada. From euclidean to minkowski space with the cauchy-riemann equations. European Physical Journal C, 56:557-569, 2008. doi:10.1140/epjc/s10052-008-0676-5. URL https://doi.org/10.1140/epjc/s10052-008-0676-5.
- [26] Markus Q. Huber, Wolfgang J. Kern, and Reinhard Alkofer. Analytic structure of three-point functions from contour deformations. Phys. Rev. D, 107:074026, Apr 2023. doi:10.1103/PhysRevD.107.074026. URL https://link.aps.org/ doi/10.1103/PhysRevD.107.074026.
- [27] Gernot Eichmann, Pedro Duarte, M. T. Peña, and Alfred Stadler. Scattering amplitudes and contour deformations. Phys. Rev. D, 100:094001, Nov 2019. doi:10.1103/PhysRevD.100.094001. URL https://link.aps.org/doi/10.1103/PhysRevD.100.094001.
- [28] Vladimír Šauli. Minkowski solution of dyson–schwinger equations in momentum subtraction scheme. J. High Energy Phys., 2003(02):001, 2003. doi:10.1088/1126-6708/2003/02/001.
- [29] Andreas Blumhofer and Jürgen Manus. New insight in dynamical symmetry breaking via imaginary part analysis. *Nucl. Phys. B*, 515:522–548, 1998. doi:10.1016/S0550-3213(98)00017-1.
- [30] David Atkinson and J. C. R. Bloch. Qcd in the infrared with exact angular integrations. Mod. Phys. Lett. A, 13:1055–1064, 1998. doi:10.1142/S0217732398001119.
- [31] Reijiro Fukuda and Taichiro Kugo. Schwinger-dyson equation for massless vector theory and the absence of a fermion pole. Nuclear Physics B, 117(1):250-264, 1976. ISSN 0550-3213. doi:10.1016/0550-3213(76)90572-1. URL https://www.sciencedirect.com/science/article/pii/0550321376905721.
- [32] G.V. Efimov. Non-local quantum theory of the scalar field. Communications in Mathematical Physics, 5:42-56, 1967. doi:10.1007/BF01646357. URL https://doi.org/10.1007/BF01646357.
- [33] John M. Cornwall and Joannis Papavassiliou. Gauge invariant three-gluon vertex in qcd. *Phys. Rev. D*, 40:3474–3483, 1989. doi:10.1103/PhysRevD.40.3474.
- [34] Daniele Binosi and Joannis Papavassiliou. Gauge-independent off-shell fermion self-energies at two loops: the cases of qed and qcd. Phys. Rev. D, 65:085003, 2002. doi:10.1103/PhysRevD.65.085003.
- [35] Ansgar Denner, Stefan Dittmaier, and Gerhard Weiglein. Application of the background field method to the electroweak standard model. *Nucl. Phys. B*, 440:95–128, 1995. doi:10.1016/0550-3213(95)00037-S.
- [36] Orlando Oliveira, Helena Lessa Macedo, and Rodrigo Carmo Terin. Looking at qed with dyson–schwinger equations: Basic equations, ward–takahashi identities and the two-photon–two-fermion irreducible vertex. Few Body Syst., 64(3):67, 2023. doi:10.1007/s00601-023-01846-5.
- [37] Isaac E. Lagaris, Aristidis Likas, and Dimitrios I. Fotiadis. Artificial neural networks for solving ordinary and partial differential equations. IEEE Trans. Neural Netw., 9(5):987–1000, 1998. doi:10.1109/72.712178.
- [38] Maziar Raissi, Paris Perdikaris, and George E. Karniadakis. Physics-informed neural networks: A deep learning framework for solving forward and inverse problems involving nonlinear partial differential equations. J. Comput. Phys., 378:686-707, 2019. doi:10.1016/j.jcp.2018.10.045.

- [39] George E. Karniadakis, Ioannis G. Kevrekidis, Lu Lu, Paris Perdikaris, Sifan Wang, and Liu Yang. Physics-informed machine learning. *Nat. Rev. Phys.*, 3:422–440, 2021. doi:10.1038/s42254-021-00314-5.
- [40] Maziar Raissi, Paris Perdikaris, and George E. Karniadakis. Hidden fluid mechanics: Learning velocity and pressure fields from flow visualizations. *Science*, 367(6481):1026–1030, 2020. doi:10.1126/science.aaw4741.
- [41] Georgios Kissas, Yibo Yang, Ehsan H. H. Kim, William R. H. Magland, Paris Perdikaris, and Michael A. G. Fernández. Machine learning in cardiovascular flows modeling: Predicting arterial blood pressure from non-invasive 4d flow mri data using physics-informed neural networks. Comput. Methods Appl. Mech. Eng., 358:112623, 2020. doi:10.1016/j.cma.2019.112623.
- [42] Jacob Mathews, Marco Francisquez, John W. Hughes, Daniel R. Hatch, Bei Zhu, and Ben J. Rogers. Uncovering turbulent plasma dynamics via deep learning from partial observations. *Phys. Rev. E*, 104(2):025205, 2021. doi: 10.1103/PhysRevE.104.025205.
- [43] David Pfau, James S. Spencer, Alexander G. D. G. Matthews, and W. M. C. Foulkes. Ab initio solution of the many-electron schrödinger equation with deep neural networks. *Phys. Rev. Res.*, 2(3):033429, 2020. doi: 10.1103/PhysRevResearch.2.033429.
- [44] Linfeng Zhang, Jiequn Han, Han Wang, Roberto Car, and Weinan E. Deep potential molecular dynamics: A scalable model with the accuracy of quantum mechanics. *Phys. Rev. Lett.*, 120:143001, 2018. doi:10.1103/PhysRevLett.120.143001.
- [45] Liu Yang, Xuhui Meng, and George E. Karniadakis. B-pinns: Bayesian physics-informed neural networks for forward and inverse pde problems with noisy data. *J. Comput. Phys.*, 425:109913, 2021. doi:10.1016/j.jcp.2020.109913.
- [46] Ameya D. Jagtap and George E. Karniadakis. Extended physics-informed neural networks (xpinns): A generalized space-time domain decomposition based deep learning framework for nonlinear partial differential equations. Commun. Comput. Phys., 28(5):2002–2041, 2020. doi:10.4208/cicp.OA-2020-0164.
- [47] Lu Lu, Pengzhan Jin, Guofei Pang, Zhongqiang Zhang, and George E. Karniadakis. Learning nonlinear operators via deeponet based on the universal approximation theorem of operators. *Nat. Mach. Intell.*, 3:218–229, 2021. doi:10.1038/s42256-021-00302-5.
- [48] Xuhui Meng and George E. Karniadakis. A composite neural network that learns from multi-fidelity data: Application to function approximation and inverse pde problems. J. Comput. Phys., 401:109020, 2020. doi:10.1016/j.jcp.2019.109020.
- [49] Lorenzo Brevi, Antonio Mandarino, and Enrico Prati. Addressing the non-perturbative regime of the quantum anharmonic oscillator by physics-informed neural networks. New J. Phys., 26(10):103015, 2024. doi:10.1088/1367-2630/ad7e2e.
- [50] Lorenzo Brevi, Antonio Mandarino, and Enrico Prati. A tutorial on the use of physics-informed neural networks to compute the spectrum of quantum systems. *Technologies*, 12(10):174, 2024. doi:10.3390/technologies12100174.
- [51] Yongji Wang, Mehdi Bennani, James Martens, Sébastien Racanière, Sam Blackwell, Alex Matthews, Stanislav Nikolov, Gonzalo Cao-Labora, Daniel S. Park, Martin Arjovsky, Daniel Worrall, Chongli Qin, Ferran Alet, Borislav Kozlovskii, Nenad Tomašev, Alex Davies, Pushmeet Kohli, Tristan Buckmaster, Bogdan Georgiev, Javier Gómez-Serrano, Ray Jiang, and Ching-Yao Lai. Discovery of unstable singularities, 2025. URL https://arxiv.org/abs/2509.14185.
- [52] Rodrigo Carmo Terin. Physics-informed neural networks viewpoint for solving the dyson-schwinger equations of quantum electrodynamics. *SciPost Phys. Core*, 8:054, 2025. doi:10.21468/SciPostPhysCore.8.3.054. URL https://scipost.org/10.21468/SciPostPhysCore.8.3.054.
- [53] Rodrigo Carmo Terin. The GINN framework: a stochastic QED correspondence for stability and chaos in deep neural networks. 8 2025.
- [54] Pedro Lima and Teresa Diogo. An extrapolation method for a volterra integral equation with weakly singular kernel. Applied Numerical Mathematics, 24(2):131-148, 1997. ISSN 0168-9274. doi:https://doi.org/10.1016/S0168-9274(97)00016-0. URL https://www.sciencedirect.com/science/article/pii/S0168927497000160. Second International Conference on the Numerical Solution of Volterra and Delay Equations.
- [55] Gobinda Rakshit, Akshay S. Rane, and Kshitij Patil. Richardson extrapolation for the iterated galerkin solution of urysohn integral equations with green's kernels. *International Journal of Computer Mathematics*, 99(8):1538-1556, 2022. doi:10.1080/00207160.2021.1986215. URL https://doi.org/10.1080/00207160.2021.1986215.
- [56] Kenneth G. Wilson. Confinement of quarks. Phys. Rev. D, 10:2445-2459, Oct 1974. doi:10.1103/PhysRevD.10.2445. URL https://link.aps.org/doi/10.1103/PhysRevD.10.2445.
- [57] John B. Kogut. An introduction to lattice gauge theory and spin systems. Rev. Mod. Phys., 51:659-713, Oct 1979. doi:10.1103/RevModPhys.51.659. URL https://link.aps.org/doi/10.1103/RevModPhys.51.659.
- [58] Michael Creutz. Monte carlo study of quantized su(2) gauge theory. Phys. Rev. D, 21:2308-2315, Apr 1980. doi: 10.1103/PhysRevD.21.2308. URL https://link.aps.org/doi/10.1103/PhysRevD.21.2308.
- [59] Shaozhi Li, Philip M. Dee, Ehsan Khatami, and Steven Johnston. Accelerating lattice quantum monte carlo simulations using artificial neural networks: Application to the holstein model. *Phys. Rev. B*, 100:020302, Jul 2019. doi: 10.1103/PhysRevB.100.020302. URL https://link.aps.org/doi/10.1103/PhysRevB.100.020302.
- [60] E. E. Salpeter and H. A. Bethe. A relativistic equation for bound-state problems. *Phys. Rev.*, 84:1232–1242, Dec 1951. doi:10.1103/PhysRev.84.1232. URL https://link.aps.org/doi/10.1103/PhysRev.84.1232.